

# Fano-type Effect in Hydrogen-Terminated Pure Nanodiamond

Oleg S. Kudryavtsev, Rustem H. Bagramov, Arkady M. Satanin, Andrey A. Shiryaev, Oleg I. Lebedev, Alexey M. Romshin, Dmitrii G. Pasternak, Alexander V. Nikolaev, Vladimir P. Filonenko, and Igor I. Vlasov\*



Cite This: <https://doi.org/10.1021/acs.nanolett.1c04887>



Read Online

ACCESS |



Metrics & More



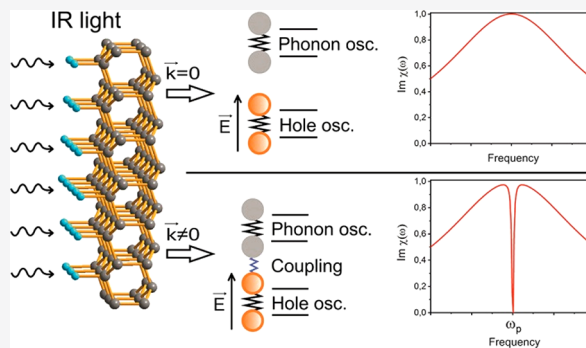
Article Recommendations



Supporting Information

**ABSTRACT:** Two novel properties, unique for semiconductors, a negative electron affinity and a high p-type surface electrical conductivity, were discovered in diamond at the end of the last century. Both properties appear when the diamond surface is hydrogenated. A natural question arises: is the influence of the surface hydrogen on diamond limited only to the electrical properties? Here, for the first time to our knowledge, we observe a transparency peak at  $1328\text{ cm}^{-1}$  in the infrared absorption of hydrogen-terminated pure (undoped) nanodiamonds. This new optical property is ascribed to Fano-type destructive interference between zone-center optical phonons and free carriers (holes) appearing in the near-surface layer of hydrogenated nanodiamond. This work opens the way to explore the physics of electron–phonon coupling in undoped semiconductors and promises the application of H-terminated nanodiamonds as a new optical material with induced transparency in the infrared optical range.

**KEYWORDS:** nanodiamond, Fano interference, transfer doping, IR absorption, Raman scattering



The surface electrical conductivity in diamonds is explained using the model of electrochemical “transfer doping”, in which an electron density transfer occurs from the hydrogen-terminated diamond surface into, for example, an adsorbed water layer, causing a charge dipole, resulting in hole accumulation and an upward band bending of the valence band maximum near the diamond surface.<sup>1</sup> Transfer doping of diamond generates hole carriers with a typical concentration of  $10^{12}$ – $10^{13}\text{ cm}^{-2}$ .<sup>2,3</sup> Taking into account that a typical width of near-surface layers does not exceed 1 nm,<sup>4</sup> one obtains a relatively high bulk concentration of free charge carriers  $10^{19}$ – $10^{20}\text{ cm}^{-3}$ . It is known that at such high concentrations of free carriers in doped semiconductors one can observe Fano-type interference<sup>5,6</sup> between the discrete states of optical phonons and the continuum of electron (hole) states induced by substitutional impurities. This interference manifests itself in an asymmetric profile of phonon lines in Raman spectra of heavily doped semiconductors, including boron-doped diamonds.<sup>7–11</sup> The Fano effect has been observed earlier also in IR absorption of silicon and germanium containing a large concentration of acceptor impurities.<sup>12–14</sup> It is natural to suggest analogous Fano-type interference in the near-surface region of highly hydrogenated diamond, containing a large concentration of free carriers. In the absence of conventional dopants, its lattice remains perfect, ensuring a high  $Q$ -factor of the phonon oscillator and, subsequently, enhancing the effect of Fano interference. The choice of nanosized diamond

possessing an increased surface-to-volume ratio creates favorable conditions for the experimental detection of the Fano interference. Nevertheless, so far there have been no reports on the electron–phonon interaction, neither on Raman scattering nor on IR absorption of hydrogenated nanodiamond (ND). The main reasons for the lack of such works are assumed to be widespread use of highly defective detonation NDs, containing a large amount of nitrogen impurities and structural defects, as well as the insufficiently high efficiency of ND surface hydrogenation by thermochemical treatment.<sup>15</sup>

In the present work, to detect the Fano-type interference, we employ a new generation of nanodiamonds produced from hydrocarbons under high pressure and high temperature (HPHT) (see Methods). As has been shown earlier<sup>16,17</sup> and confirmed in the present work, the surfaces of ND particles synthesized from hydrocarbon compounds are effectively terminated by hydrogen. This is evidenced by the observation of  $\text{CH}_x$  phonon modes in Raman, which are never detected in NDs hydrogenated thermochemically.

**Received:** July 5, 2021

**Revised:** March 9, 2022

Diamond crystallite sizes were determined by transmission electron microscopy (TEM) (Figure 1a) and X-ray diffraction

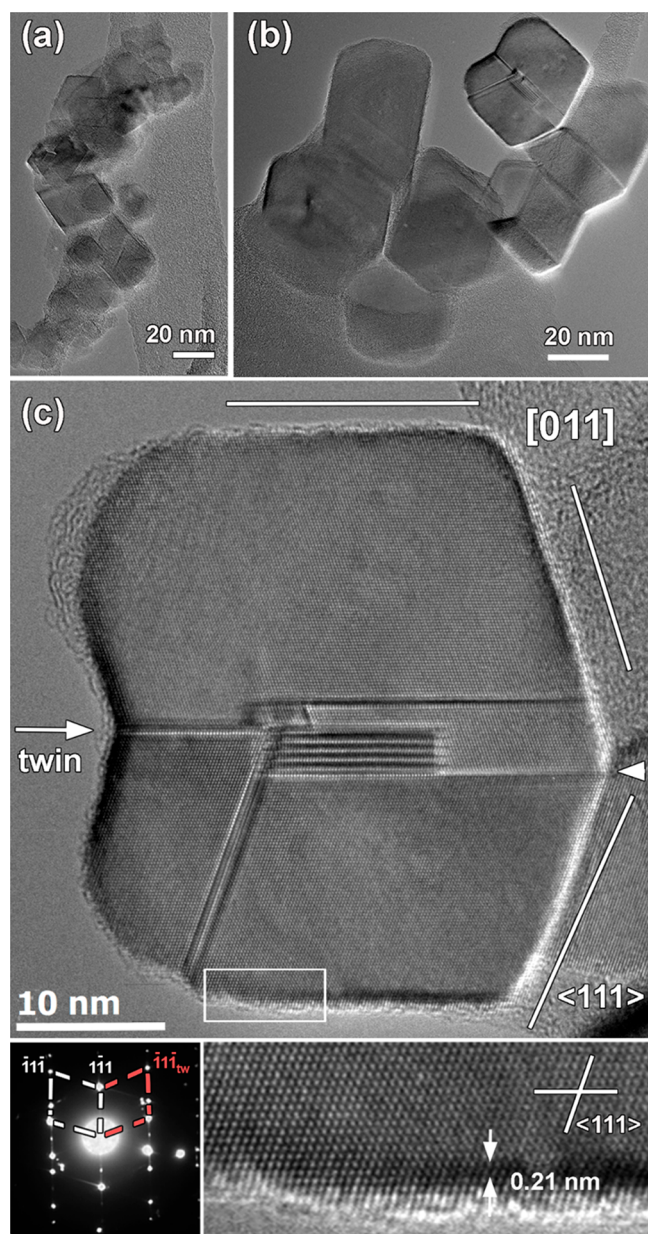


**Figure 1.** TEM images of the nanodiamonds. (a) BF low magnification overview TEM image of the ND sample, (b) low magnification TEM image of highly twinned NDs, (c) [011] HRTEM image of one of the twinned crystallites shown in (b). The corresponding twin ED pattern is shown in the bottom left panel. Matrix and twin spots are depicted with white and red boxes, respectively. The magnified image of the near-surface region selected in (c) is shown in the bottom right panel.

analysis (Figure 1S in Supporting Information, section S1). TEM studies show that characteristic sizes of diamond nanocrystals vary in the range of 20–40 nm (Figure 1a), although crystals  $\sim 1 \mu\text{m}$  are occasionally encountered. Many diamonds tend to twin along the  $\langle 111 \rangle$  plane (Figure 1b,c). High-resolution TEM images show a perfect lattice,  $\{111\}$  morphology (Figure 1c), and sharp and clean surfaces of diamond crystallites (Figure 1c inset).

Crystal sizes of about 30 nm are supposed to be optimal for determining the Fano-type interference in hydrogenated diamond. An unusually bright SEM image of 30 nm NDs (Figure S2 in Supporting Information, section S2) indicates a noticeable negative electron affinity of their surfaces. As shown by Bolker et al.,<sup>3</sup> smaller particles appear less promising since they can have weaker negative electron affinity and lower near-surface hole concentration.

Raman and IR absorption spectroscopies were used to determine the Fano-type interference in the ND sample.

In the Raman spectrum, a slight asymmetry in the diamond line profile centered at  $1332 \text{ cm}^{-1}$  was observed (Figure 2a). This asymmetry is associated with the Fano interference between optical phonons and holes in the near-surface diamond layer. However, as we can see, for 30 nm diamond particles, the contribution of this layer is relatively small, and the interference is masked by the intense symmetric peak of bulk optical phonons. Thus, a detailed analysis of expected interference turns out to be inaccessible in Raman spectroscopy.

Upon annealing the sample in air at  $400 \text{ }^\circ\text{C}$  (see Methods), a major fraction of the hydrogen is removed from the ND surfaces (see Supporting Information, section S3), and the resulting diamond line is well fitted by the symmetric Lorentz profile (the inset of Figure 2a). This experiment confirms that the profile asymmetry is directly related to the hydrogen-terminated ND surface.

The IR absorption spectrum of our sample is shown in Figure 2b. Its main features are

- the narrow dip in absorption (transparency peak) at frequency  $1328 \text{ cm}^{-1}$ ,
- the intense band of  $\text{CH}_x$  vibration modes in the range  $2800\text{--}3000 \text{ cm}^{-1}$ ,
- the background absorption steadily increasing toward low frequencies (starting from  $6000 \text{ cm}^{-1}$ ).

The absence of characteristic C–F bond absorption within  $1100\text{--}1300 \text{ cm}^{-1}$ <sup>18,19</sup> implies the absence of fluorine (from the precursor) on diamond surfaces. Upon annealing of the sample in air at  $400 \text{ }^\circ\text{C}$  (see Methods) for 30 min, a substantial drop of the  $\text{CH}_x$  absorption is accompanied by a decrease in the wide-band absorption and the transparency peak. Similar to the changes in Raman, these changes demonstrate the direct relation of the transparency peak and the background absorption to the hydrogen-terminated ND surface.

For comparison, Raman and IR absorption spectra of 30 nm diamond particles with chemically oxidized surface (Tomei Diamond Co. Ltd., Japan) were recorded before and after annealing at  $400 \text{ }^\circ\text{C}$ . The symmetry and width of the diamond line at  $1332 \text{ cm}^{-1}$  were found to remain unchanged during annealing (Figure 4Sa in Supporting Information, section S4). The IR absorption spectra of the nanodiamonds do not exhibit either the temperature-dependent background absorption or the narrow transparency peak at  $1328 \text{ cm}^{-1}$  (Figure 4Sb in Supporting Information, section S4). This comparison once again confirms the relation of the features in the Raman and IR spectra observed in Figure 2 to the hydrogen-terminated ND surface.

Now we turn to the interpretation of the main features detected in the absorption spectrum of the pristine sample. We attribute the wide-band absorption to the continuum of hole states and the transparency peak at  $1328 \text{ cm}^{-1}$  to the destructive interference between the holes and zone-center

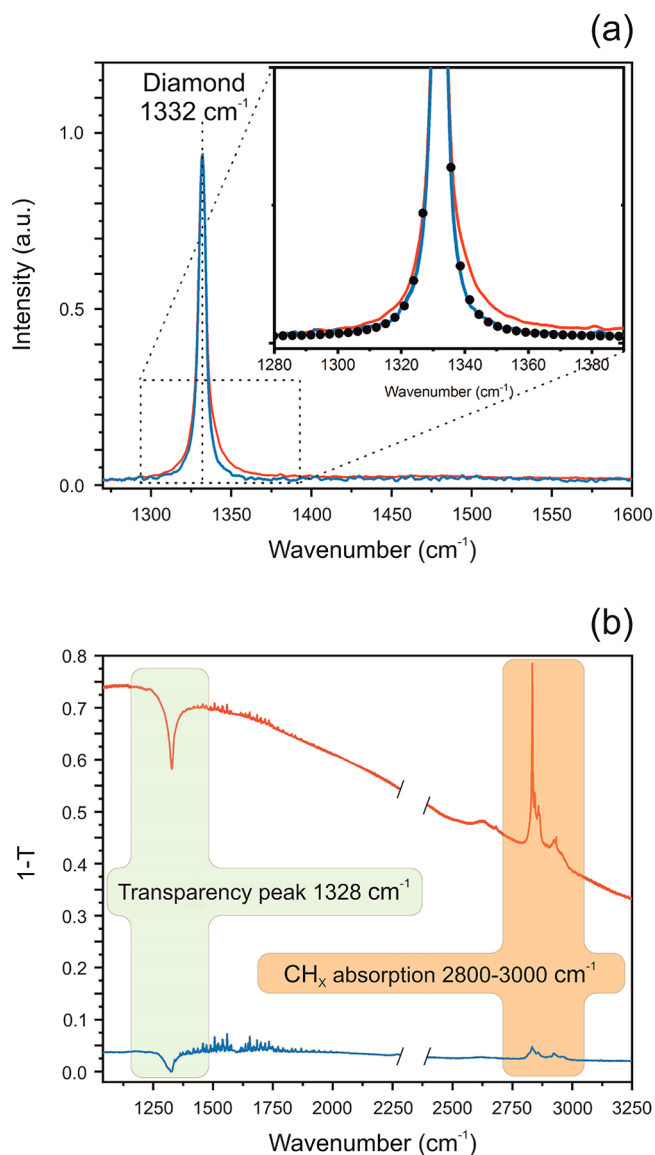


**Figure 2.** Raman and IR absorption spectra of the sample. (a) Room-temperature Raman spectra of the initial (red curve) and annealed at 400 °C (blue curve) samples. The spectra are characterized by a narrow diamond line at 1332  $\text{cm}^{-1}$ . The inset demonstrates asymmetry of the initial diamond line. After annealing, the diamond line is well fitted by the Lorentz profile indicated by black dots. (b) IR absorption spectra (in units 1-T, where T is transmittance) measured at room temperature for the initial (red curve) and annealed at 400 °C (blue curve) samples. The spectra are corrected for the scattering losses at 6000  $\text{cm}^{-1}$  on the assumption that the losses are constant in the range 1000–6000  $\text{cm}^{-1}$ . A narrow dip (transparency peak) at 1328  $\text{cm}^{-1}$  is related to the Fano-type destructive interference between phonons and holes. The omitted region around 2370  $\text{cm}^{-1}$  contains uncompensated atmospheric  $\text{CO}_2$  absorption. The structured band within 2800–3000  $\text{cm}^{-1}$  is due to  $\text{CH}_x$  vibration modes. The background absorption, steadily increasing toward low frequencies, is attributed to free carriers. Note a considerable decrease of the 1328  $\text{cm}^{-1}$  dip and a marked reduction of the background level after the main fraction of hydrogen is removed.

optical phonons. The closest analogue of this interference is the effect of coupled-resonator-induced transparency (CRIT).<sup>20–23</sup> In CRIT, the destructive interference is a result of an internal coupling between individual resonators. In our case, we deal with the phonon-hole coupling. The important

condition for the manifestation of the CRIT effect is a difference in resonator losses. The CRIT resonator non-interacting with the external field should have considerably smaller losses in comparison with the interacting one. Similarly, the  $Q$ -factor of the phonon oscillator (noninteracting with the external field) is demonstrated to be much higher than the hole one (see Supporting Information, section S6).

Below we describe the nature of the phonon-hole interference in terms of “phonon” and “hole” oscillators. On the basis of the microscopic approach, the hole oscillator is interpreted as the excitation of a virtual electronic state above the Fermi level and a hole state below the Fermi level upon absorption of an infrared photon.<sup>24</sup> Such excitation becomes possible upon strong transfer doping of diamond, which results in the valence band bending above the Fermi level in a near-surface layer of the ND crystals. The hole oscillator is described within the plasmonic model (see Supporting Information, section S5) with the amplitude  $A_h$ , the eigenfrequency  $\omega_h$  and the damping coefficient  $\gamma_h$ . This oscillator is excited by an incoming electromagnetic field with the amplitude  $E$ . The optical phonon oscillator is described within the Einstein model (see Supporting Information, section S5) with the amplitude  $A_p$ , the eigenfrequency  $\omega_p$ , and the damping coefficient  $\gamma_p$ . As we have already mentioned,  $\gamma_p \ll \gamma_h$ . In the range of resonance frequencies,  $\omega \approx \omega_h \sim \omega_p$ , the approximate equations for the amplitudes of the coupled oscillators in the external field (see details in Supporting Information, section S5) are given by

$$\begin{aligned} (\delta_h + i\gamma_h/2)A_h + \bar{k}A_p &= A_{\text{in}} \\ \bar{k}A_h + (\delta_p + i\gamma_p/2)A_p &= 0 \end{aligned} \quad (1)$$

where  $\bar{k} = k/2\omega_h$  and  $k$  is the coupling coefficient of the oscillators,  $\delta_h = \omega - \omega_h$  and  $\delta_p = \frac{\omega_h^2 - \omega_p^2}{2\omega_h} + \delta_h$  are the frequency detuning parameters,  $A_{\text{in}} = \frac{e}{2\omega_h m_h} E$  is the driving amplitude.

Expressing the dielectric susceptibility in terms of the amplitude ratio  $\frac{A_h}{A_{\text{in}}}$  and solving eq 1 in the limit  $\gamma_p \rightarrow 0$ , we obtain the following dependence of the imaginary part of the dielectric susceptibility  $\text{Im}\chi(\omega)$ , describing the absorption of two interacting oscillators, on the external field frequency:

$$\text{Im}\chi(\omega) = \frac{e^2 n}{2\omega_p m_h \epsilon_d \epsilon_0} \frac{\gamma_h/2}{(\gamma_h/2)^2 + (\delta_h - \bar{k}^2/\delta_p)^2} \quad (2)$$

where  $n$  is the hole concentration in the near-surface diamond layer, and  $m_h$  is the hole mass.

The  $\text{Im}\chi(\omega)$  profiles are analyzed for 2 main regimes:

- (i) The oscillators are uncoupled,  $k = 0$ , and then  $\text{Im}\chi(\omega)$  is described by a wide Lorentz profile, shown in Figure 3a. The phonon oscillator is completely decoupled from the hole oscillator and forms a so-called “dark state”.
- (ii) The oscillators are weakly coupled; i.e.,  $\bar{k}$  is small but not equal to zero. In that case, when  $\delta_p \rightarrow 0$ ,  $\text{Im}\chi(\omega) \rightarrow 0$ , and a sharp dip appears in the wide absorption profile at  $\omega_p$  (Figure 3b). This regime is most consistent with our experimental observations.

In the strong-coupling limit ( $\bar{k} \gg 0$ ), the absorption profile splits into two bands well separated in frequency. It means that in the absence of damping, the eigenmodes of the oscillators

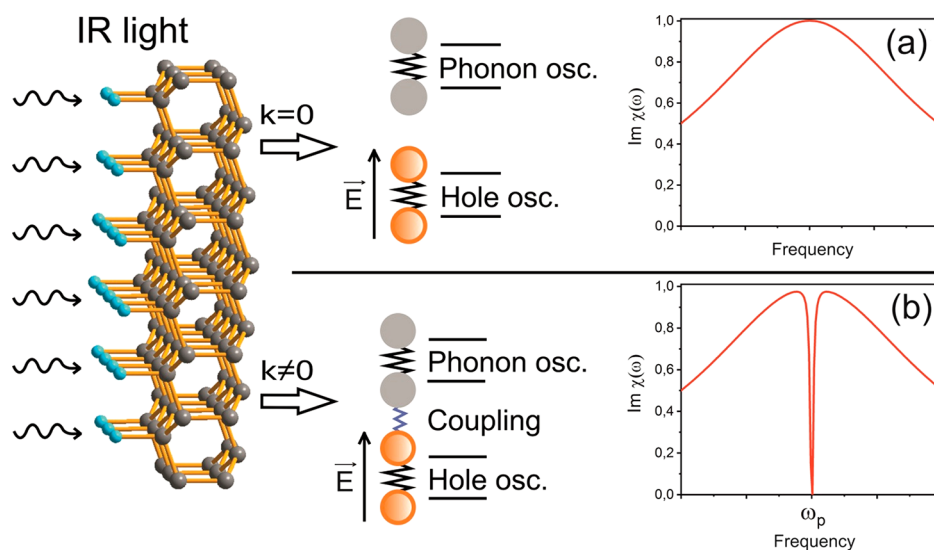


**Figure 3.** Qualitative picture of the phonon-hole interference in H-terminated diamond. Two regimes of the oscillator excitation by an incoming electromagnetic field  $E$  are shown: (a) When the phonon and hole oscillators are decoupled, the Lorentz absorption profile is caused by hole excitations, while the phonon oscillator remains “dark”. (b) With the coupling between the oscillators, the phonon oscillator compensates for dissipation losses of the hole oscillator in a narrow frequency range near the optical phonon frequency, causing a narrow dip in the Lorentz absorption profile.

strongly depend on the coupling constant  $k$ . We believe that such strongly coupled polaritonic excitations cannot be realized in nonpolar covalent crystals.

The model proposed here for the explanation of the dip in absorption is simplified, but it reflects the main features of Fano-type destructive interference. The fitting of the experimental dip in the absorption spectrum (see [Supporting Information](#), section S5) determines its position at  $1328\text{ cm}^{-1}$  and the width of  $30\text{ cm}^{-1}$ . As follows from [Figure 2b](#), the dip amounts to one-fifth of the absorption level in its neighborhood. Numerical analysis of expression (2) and the more general one (7S), obtained at  $\gamma_p \neq 0$ , shows that the width of the dip depends mainly on the coupling coefficient  $k$ , where as its depth depends on the value of phonon damping coefficient  $\gamma_p$ . The dip broadens and weakens with increasing  $k$  and  $\gamma_p$ , respectively. Our investigation of the destructive interference depending on nanodiamond sizes is in progress.

Further, we discuss the features of the Fano resonance manifestation in the IR absorption and Raman scattering of hydrogenated nanodiamond. In the IR absorption of hydrogenated nanodiamond, we are dealing with a specific Fano-type effect (analogue of coupled-resonator-induced transparency<sup>23</sup>), when the external electromagnetic field interacts with only one (hole) of two coupled oscillators. Since the Fano parameter  $q$  characterizes the ratio of the probabilities of transition to a discrete state and to a continuum, then  $q \rightarrow 0^5$  regardless of the ratio between the frequencies  $\omega_h$  and  $\omega_p$ , and the Fano dip will be kept as long as the frequency of the optical phonon lies in the band of resonant frequencies of holes (exactly what we see in [Figure 2b](#)). Our experiment with the sample annealing demonstrates that no visible changes happen in the transparency peak profile when we shift frequencies  $\omega_h$  relative to  $\omega_p$ . Indeed, upon annealing, the concentration of hydrogen on the diamond surface decreases, and hence the concentration of holes in the near-surface layer also decreases. This decreases the resonant frequencies of hole oscillators and the absorption intensity at a frequency of optical phonons. Nevertheless, the

line shape of the transparency peak does not change noticeably.

In contrast to IR absorption, in the Raman scattering, an external electromagnetic field interacts with both phonon and hole oscillators, which allows the parameter  $q$ , and hence the Fano profile, to vary widely. By analogy with heavily boron-doped diamond (the resonant frequency of the hole oscillator is in IR), for which an asymmetric line shape is observed in the Raman spectrum upon visible light excitation,<sup>10,11</sup> we could expect a similar asymmetry for the hydrogenated diamond. However, because of the small near-surface region of the hole-phonon interaction with respect to the volume of 30 nm diamond, we are able to discern only a slight asymmetry of the Raman line ([Figure 2a](#)).

In conclusion, we have found a narrow dip at the frequency  $1328\text{ cm}^{-1}$  in the IR absorption spectra of 30 nm H-terminated diamond particles synthesized at high pressure. We relate this effect, unusual for pure diamond, to the destructive interference of the Fano-type between zone-center phonons and free charge carriers appearing in the near-surface layer of the hydrogenated nanodiamond. The destructive interference is explained by a simple model of two coupled oscillators, one of which interacts with the external electromagnetic field. Provided that a high local concentration of holes is reached in the hydrogen-terminated nanodiamond, we could speculate that such NDs could be superconducting similar to diamond doped with boron at the level  $>10^{21}\text{ cm}^{-3}$ .<sup>25</sup> A sharp dip in the absorption near the optical phonon frequency gives rise to an anomalous light dispersion in this region. Materials with this property are able to reduce the group velocity of the transmitted light.<sup>26</sup> Thus, the hydrogenated nanodiamond represents a new optically active media which can be used for controlling the velocity of IR light pulses. “Slowed” light is currently employed in the optical buffers,<sup>27</sup> quantum networks,<sup>28</sup> and quantum memory.<sup>29</sup> On the whole, finding the IR transparency peak induced by phonon-hole coupling opens a new page in investigation and application of diamond in the infrared optical range.

## METHODS

### Nanodiamonds Synthesis and Sample Preparation.

Nanodiamonds were synthesized from a mixture of adamantane (C<sub>10</sub>H<sub>16</sub>, Aldrich, 99% purity) and octafluoronaphthalene (C<sub>10</sub>F<sub>8</sub>, Alpha Aesar, 96% purity), which were manually mixed in an agate mortar (the octafluoronaphthalene/adamantane weight ratio was 1/4). The mixture was placed in a titanium capsule and then in a graphite heater inside a lithographic stone container. For treatment at 7.5 GPa and 1400 °C, an apparatus of toroidal-type was used.<sup>30</sup> The synthesized ND is a white powder with a bluish hint. Because of their hydrophobicity, ND particles are poorly dispersed in water, and upon drying of a ND suspension on a substrate they form agglomerates of various sizes.

**Sample Annealing.** Samples were annealed in the air in a LinKam TS1500 chamber at a constant temperature of 400 °C for varied time intervals. The heating rate was 120 °C/min. Raman and IR absorption spectra were recorded after cooling to room temperature. At the preliminary stage of our research, it was found that the main changes in those spectra occur within 30 min of annealing. Therefore, in the main text the results on the sample annealing are given for a 30 min annealing time (see Figures 2 and S3). With a further increase in the annealing time, the changes in the spectra are significantly slowed down. This is because the spectra are recorded for a large agglomerate of diamond nanoparticles. As a result, oxygen effectively interacts only with the outer layer of such an agglomerate, and the particles in the center of the agglomerate remain hydrogenated for a longer time.

**Raman Spectroscopy.** Raman spectra of the nanodiamonds were recorded at room temperature with a LABRAM HR800 spectrometer equipped with a 473 nm diode laser. The exciting laser radiation of the power 10 mW was focused on samples by means of a 100× Olympus lens and NA = 0.95. The scattered radiation was registered in the backscattering geometry.

**IR Absorption Spectroscopy.** IR absorption spectra of the nanodiamonds were recorded at room temperature using an IR microscope Thermo Fisher Scientific Nicolet iN10. The spectra were recorded in the mid-infrared range 1000–6000 cm<sup>-1</sup> with a resolution of 2 cm<sup>-1</sup>. In the absorption mode, the samples were dispersed on a KBr pellet and measured with square apertures ranging from 30 to 150 μm depending on the size of the ND agglomerates. In addition, reflectance spectra from samples dispersed on Al or Au mirrors were studied. As expected, the 1328 cm<sup>-1</sup> feature changes sign in the reflectance spectra.

**TEM Analysis.** Transmission electron microscopy (TEM) was performed using a JEM ARM200F cold FEG double aberration corrected microscope, operated at 200 kV and equipped with a large-angle CENTURIO EDX detector, OriusGatan CCD camera, and Quantum GIF. The TEM samples were prepared in a conventional way, by depositing a solution of the material on holey carbon-supported copper grids.

## ASSOCIATED CONTENT

### Supporting Information

The Supporting Information is available free of charge at <https://pubs.acs.org/doi/10.1021/acs.nanolett.1c04887>.

Detailed description of X-ray diffraction analysis and scanning electron microscopy of the sample, Raman spectra of C–H vibration modes, phonon-hole interfer-

ence, Q-factor estimation for the phonon and hole oscillators (PDF)

## AUTHOR INFORMATION

### Corresponding Author

Igor I. Vlasov – Prokhorov General Physics Institute of the Russian Academy of Sciences, 119991 Moscow, Russia; [orcid.org/0000-0002-0971-8495](https://orcid.org/0000-0002-0971-8495); Email: [vlasov@nsc.gpi.ru](mailto:vlasov@nsc.gpi.ru)

### Authors

Oleg S. Kudryavtsev – Prokhorov General Physics Institute of the Russian Academy of Sciences, 119991 Moscow, Russia

Rustem H. Bagramov – Vereshchagin Institute of High Pressure Physics, Russian Academy of Sciences, 108840 Moscow, Russia

Arkady M. Satanin – Dukhov All-Russia Research Institute of Automatics, 127030 Moscow, Russia; National Research University Higher School of Economics, 101000 Moscow, Russia

Andrey A. Shiryaev – Frumkin Institute of Physical Chemistry and Electrochemistry RAS, 119071 Moscow, Russia

Oleg I. Lebedev – Laboratoire CRISMAT, UMR 6508 CNRS-ENSICAEN, 14050 Caen, France

Alexey M. Romshin – Prokhorov General Physics Institute of the Russian Academy of Sciences, 119991 Moscow, Russia

Dmitrii G. Pasternak – Prokhorov General Physics Institute of the Russian Academy of Sciences, 119991 Moscow, Russia

Alexander V. Nikolaev – Skobeltsyn Institute of Nuclear Physics Lomonosov Moscow State University, 119991 Moscow, Russia; School of Electronics, Photonics and Molecular Physics, Moscow Institute of Physics and Technology, 141700 Dolgoprudny, Russia; [orcid.org/0000-0003-1420-5181](https://orcid.org/0000-0003-1420-5181)

Vladimir P. Filonenko – Vereshchagin Institute of High Pressure Physics, Russian Academy of Sciences, 108840 Moscow, Russia

Complete contact information is available at:

<https://pubs.acs.org/10.1021/acs.nanolett.1c04887>

### Notes

The authors declare no competing financial interest.

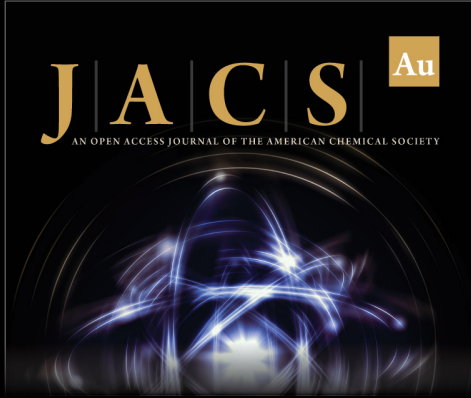
## ACKNOWLEDGMENTS

A.M.S. acknowledges support from the RSF Grant No. 22-21-00586. X-ray diffraction and IR microscopy were performed using the equipment of the Center of Shared Use of IPCE RAS.

## REFERENCES


- (1) Maier, F.; Riedel, M.; Mantel, B.; Ristein, J.; Ley, L. Origin of surface conductivity in diamond. *Phys. Rev. Lett.* **2000**, *85*, 3472–3475.
- (2) Nebel, C. E. Surface electronic properties of diamond. *arXiv.org e-Print archive*, arXiv:2005.03893, <https://arxiv.org/abs/2005.03893> (accessed May 08, 2020).
- (3) Bolker, A.; Saguy, C.; Kalish, R. Transfer doping of single isolated nanodiamonds, studied by scanning probe microscopy techniques. *Nanotechnology* **2014**, *25*, 385702.
- (4) Edmonds, M. T.; Pakes, C. I.; Ley, L. Self-consistent solution of the Schrödinger-Poisson equations for hydrogen terminated diamond. *Phys. Rev. B* **2010**, *81*, 085314.


- (5) Fano, U. Effects of Configuration Interaction on Intensities and Phase Shifts. *Phys. Rev.* **1961**, *124*, 1866–1878.
- (6) Joe, Y. S.; Satanin, A. M.; Kim, C. S. Classical analogy of Fano resonances. *Phys. Scr.* **2006**, *74*, 259–266.
- (7) Pruvost, F.; Deneuve, A. Analysis of the Fano in diamond. *Diamond & Related Materials* **2001**, *10*, 531–535.
- (8) Cerdeira, F.; Fjeldly, T. A.; Cardona, M. Effect of Free Carriers on Zone-Center Vibrational Modes in Heavily Doped p-type Si. II. Optical Modes. *Phys. Rev. B* **1973**, *8*, 4734–4745.
- (9) Cardona, M., Klein, M. V. *Light Scattering in Solids*; Springer: Berlin, Heidelberg, 1975; pp 148–208.
- (10) Ager, J. W., III; Walukiewicz, W.; McCluskey, M.; Plano, M. A.; Landstrass, M. I. Fano interference of the Raman phonon in heavily boron doped diamond films grown by chemical vapor deposition. *Appl. Phys. Lett.* **1995**, *66*, 616–618.
- (11) Mortet, V.; et al. Analysis of heavily boron-doped diamond Raman spectrum. *Diamond & Related Materials* **2018**, *88*, 163–166.
- (12) Humlíček, J. Ellipsometric study of Fano resonance in heavily doped p-type Si and Si Ge alloys. *Thin Solid Films* **1998**, *313–314*, 656–660.
- (13) Chandrasekhar, H. R.; Ramdas, A. K.; Rodriguez, S. Resonant interaction of acceptor states with optical phonons in silicon. *Phys. Rev. B* **1976**, *14*, 2417.
- (14) Watkins, G. D.; Fowler, W. B. Resonant interactions of optical phonons with acceptor continuum states in silicon. *Phys. Rev. B* **1977**, *16*, 4524–4529.
- (15) Krueger, A.; Lang, D. Functionality is key: recent progress in the surface modification of nanodiamond. *Adv. Funct. Mater.* **2012**, *22*, 890–906.
- (16) Kudryavtsev, O. S.; Ekimov, E. A.; Romshin, A. M.; Pasternak, D. G.; Vlasov, I. I. Structure and Luminescence Properties of Nanodiamonds Produced from Adamantane. *Phys. Status Solidi A* **2018**, *215*, 1800252.
- (17) Ekimov, E. A.; et al. High-pressure synthesis and optical properties of nanodiamonds obtained from halogenated adamantanes. *Diamond & Related Materials* **2020**, *103*, 107718.
- (18) Stuart, B. H. *Infrared Spectroscopy: Fundamentals and Applications*; John Wiley & Sons Ltd: Hoboken, 2004; p 82.
- (19) Petit, T.; Puskar, L. FTIR Spectroscopy of Nanodiamonds: Methods and Interpretation. *Diamond & Related Materials* **2018**, *89*, 52–66.
- (20) Lamb, W. E.; Retherford, R. C. Fine Structure of the Hydrogen Atom. Part II. *Phys. Rev.* **1951**, *81*, 222.
- (21) Hemmer, P. R.; Prentiss, M. G. Coupled-pendulum model of the stimulated resonance Raman effect. *J. Opt. Soc. Am. B* **1988**, *5*, 1613–1623.
- (22) Alzar, C. L. G.; Martinez, M. A. G.; Nussenzeig, P. Classical analog of electromagnetically induced transparency. *Am. J. Phys.* **2002**, *70*, 37.
- (23) Smith, D. D.; Chang, H.; Fuller, K. A.; Rosenberger, A. T.; Boyd, R. W. Coupled-resonator-induced transparency. *Phys. Rev. A* **2004**, *69*, 063804.
- (24) Yu, P. Y.; Cardona, M. *Fundamentals of Semiconductors: Physics and Materials Properties*; Springer-Verlag Berlin Heidelberg: Berlin, 2010.
- (25) Ekimov, E. A.; Sidorov, V. A.; Bauer, E. D.; Melnik, N. N.; Curro, N. J.; Thompson, J. D.; Stishov, S. M. Superconductivity in diamond. *Nature* **2004**, *428*, 542–545.
- (26) Hau, L. V.; Harris, S. E.; Dutton, Z.; Behroozi, C. H. Light speed reduction to 17 metres per second in an ultracold atomic gas. *Nature* **1999**, *397*, 594–598.
- (27) Boyd, R. W.; Gauthier, D. J. Controlling the velocity of light pulses. *Science* **2009**, *326*, 1074–1077.
- (28) Kimble, H. J. The quantum internet. *Nature* **2008**, *453*, 1023–1030.
- (29) Lukin, M. D.; Imamoglu, A. Controlling photons using electromagnetically induced transparency. *Nature* **2001**, *413*, 273–276.
- (30) Khvostantsev, L. G.; Slesarev, V. N.; Brazhkin, V. V. Toroid type high-pressure device: history and prospects. *High Pressure Research* **2004**, *24*, 371–383.



**JACS** Au  
AN OPEN ACCESS JOURNAL OF THE AMERICAN CHEMICAL SOCIETY

Editor-in-Chief  
**Prof. Christopher W. Jones**  
Georgia Institute of Technology, USA

**Open for Submissions** 

pubs.acs.org/jacsau  ACS Publications  
Most Trusted. Most Cited. Most Read.